Heliyon 8 (2022) e11540

Contents lists available at ScienceDirect

Heliyon

journal homepage: www.cell.com/heliyon

Research article

Numerical simulation for the control rod assembly drop time evaluation in a LFR

Emmanuel Maurice Arthur [a,b,c], Chaodong Zhang [a], Seth Kofi Debrah [b,c], Stephen Yamoah [b,e], Lei Wang [d,*]

[a] Key Laboratory of Neutronics and Radiation Safety, Institute of Nuclear Energy Safety Technology, Chinese Academy of Sciences, Hefei, Anhui 230031, China
[b] School of Nuclear and Allied Sciences, University of Ghana, Box AE 1, Kwabenya, Accra, Ghana
[c] Nuclear Power Institute, Ghana Atomic Energy Commission, Box LG 80, Accra, Ghana
[d] School of Computer Science, Hefei Normal University, Hefei, Anhui, 230601, China
[e] Nuclear Power Ghana, P. O. Box KA 9152, KIA-Airport-Accra, Ghana

ARTICLE INFO

Keywords:
Lead-cooled fast reactor
Lead–Bismuth Eutectic
Control rod assembly
Drop time

ABSTRACT

During scram, the Control Rod Assembly (CRA) is quickly dropped into the core and as well, if any of the operating limits are exceeded, the CRA is dropped into the core within a stipulated time to shut down the reactor power as soon as possible. In this study, the Computational Fluid Dynamics (CFD) approach was used to investigate the CRA drop dynamics of a lead-based research reactor. To simulate the flow field around the CRA in the guide tube, a 3-dimensional model of the CRA in the LBE-filled guide tube was developed and discretized; and the averaged Navier-Stokes equations coupled with the dynamic mesh method were adopted. Considering the large mesh deformation in the LBE coolant domain while the CRA drops, the recently developed FSI method in the CFX code, namely the rigid body approach, was adopted, which falls under the monolithic method. In this method, the translational CRA wall, which is partially immersed in the LBE, was set as a rigid body. It has the advantage of updating and improving the mesh quality through the mesh and re-meshing technique during the process of computation. Compared with the results of the work done in the available literature, the CFD model proved to be applicable and reliable. From the results, the inherent high density among the LBE flow characteristics had the most influence on the drop time. The mass of the CRA impacts its driving force so that the drop time reduces when the CRA mass is increased. In conclusion, the method used in this study can be applied to compute and predict significant parameters which can serve as a reference for a suitable design of the CRA and its drive mechanism in the case of modification for safety.

1. Introduction

In the nuclear reactor, the control rod assembly (CRA) is used to control the reactor power and as one of the internal structures for ensuring safety, it is used for scram. During scram, the CRA is quickly dropped into the core. Moreover, if any of the operating limits are exceeded, the CRA is dropped into the core within a stipulated time to shut down the reactor power as soon as possible. On receiving the scram signal, the CRA is released to drop into the reactor core by its weight under gravity. Thus, the drop time and falling velocity of the CRA must be estimated for safety evaluation. Remarkably, the safety requirements of a nuclear power plant include strict limitations on the maximum drop time of CRAs, which serves as a safety index for operation. For instance, in February 1995, several CRAs of the 944 MWe nuclear reactors in Daya Bay in China failed to comply with these requirements. The developer of the Daya Bay nuclear reactor, Electricite' De France, as a matter of urgency, undertook a research programme to better understand and solve the problem (Hofmann et al., 2000).

The drop time of the CRA is affected by its structural design and the coolant state as it falls (Cheng et al., 2020). The validation of the performance of the drop of the CRA is an essential aspect of the safety analysis of a nuclear power plant. Thus, developing a computer program that is able to compute the drop of the CRA is necessary for validating and improving the design of the CRA as well as its drive mechanism (Zhou et al., 2013). Theoretical studies are usually simplified and easy to use. Meanwhile, it can be very difficult and sometimes impossible to depict

* Corresponding author.
E-mail address: wanglei_petro@163.com (L. Wang).

https://doi.org/10.1016/j.heliyon.2022.e11540
Received 31 January 2022; Received in revised form 6 May 2022; Accepted 4 November 2022

the real behaviour of real phenomena with the use of the theoretical models.

These days, computers are becoming extremely powerful when it comes to the ability to mimic real scenarios. In effect computational fluid dynamics (CFD) is evolving with great capabilities to study fluid-structure interaction. With this development, theoretical studies have been useful, as models from such studies have been implemented in CFD codes for use. It is therefore imperative to develop the models from the available theoretical studies into CFD codes to improve the analysis. With respect to this, CFD analysis has proven to be a useful and convenient tool in developing innovative designs of the CRA and CRDM for reactor shutdown dynamics. As a result, several researches have been done to study the drop of the control rod using the CFD approach (Cheng et al., 2020; Hofmann et al., 2000; Huang et al., 2018; Huh et al., 2010, 2011, 2013, 2018; Kim et al., 2011, 2015; Lee et al., 2016, 2017; Profir et al., 2015, 2017; Oh et al., 2015; Rabiee and Atf, 2016; Singh et al., 2014; Son et al., 2019; Sun et al., 2014; Yoon et al., 2007).

However, these studies are mainly for second-generation reactors, specifically the Pressurized Water Reactors (PWRs). Although, for the third-generation reactors (such as the AP1000), the research experience from the second-generation reactor can be used as reference, yet the relevant research theory still needs to be improved and developed. For the fourth generation of nuclear reactor technology, especially the research on the CRA drop in the lead-cooled fast reactors (LFR), there is a lack of relevant experimental equipment as well as experience. Generally, studies on control rod drop in the non-water coolant is limited compared to that in water coolant. However, safety requirements of the water-cooled reactors are not same as the generation four (Gen IV) nuclear reactors.

Presently in this study, the dynamics of the CRA as it drops into the guide tube of the lead-cooled fast reactor is studied using the dynamic mesh technology of the CFX code, which can appropriately solve fluid boundary motion problems (Ferrini et al., 2016; Peng et al., 2012; Sui et al., 2013). This technology of CFX possess outstanding capabilities for simulating the drop behaviour of the CRA and can effectively avoid complicated theoretical derivation. Besides, it could analyse the transient coolant flow domain and ascertain vital parameters including the CRA drop time, velocity as well as coolant resistances against the CRA.

Evidently, as a Gen IV nuclear reactor, the China Lead-based fast research reactor (CLEAR-I) has high neutron flux with complex safety design and thus, study into the dynamics of the drop of its CRA is prospective and merits attention. However, according to the available literature, no work has been done on CLEAR-I on the use of CFD to analyse the drop dynamics of its CRA. This paper aims at methodologically developing a general and well-founded CRA drop CFD method that could analyse the CRA drop dynamics in varying LFR types, especially CLEAR-I, using CFX dynamic mesh technology.

2. Materials and method

2.1. Description of the CLEAR-I CRA and LBE-filled guide tube geometry

The pool-type fast reactor, CLEAR-I is an innovative Chinese technology archetype for the LFR, which uses Lead Bismuth Eutectic (LBE) as the primary coolant. The reactor technology spearheads the Chinese Academy of Sciences' (CAS) Accelerator Driven Subcritical (ADS) transformation system (Arthur et al., 2020; Wu et al., 2016). In terms of safety design, the CRA of CLEAR-I comprises seven (7) individual control rods banded in a stationary hexagonal guide tube. The instance of free fall, the CRA drops through the guide tube into the core. The mass of the active part (the part that is boron-enriched and absorbs the neutrons) of the CRA is 30 kg, which is inadequate to allow for a drop into the high-density LBE coolant. Therefore, 220 kg balanced weight (inactive part) is put above the active part of the CRA to allow for a free fall under gravity. At the initial stage of the fall, the active part of the CRA (800 mm) is immersed totally into the fluid (Arthur et al., 2020). The shape considered during the drop analysis of the CRA for simplicity, is a circular CRA initially partially immersed in a circular guide tube.

The geometry for the study considers a 3-dimensional model of the test section of the actual model of the CRA and guide tube (see Figure 1). The hexagonal shape of the guide tube is considered as circular in order to reduce the geometrical complexity and along with it, computational demand. Moreover, reducing the hexagonal shape of the CRA to circular will help to reduce or avoid the uncertainties in the simulation. In the guide tube, the CRA is initially partly (halfway) immersed in the LBE coolant. The dimensions of the guide tube and CRA is shown in Table 1. Since the geometry for the study mimics the test section of the actual model, the guide tube has an inlet at the bottom and an outlet at the top. The geometry considers the active and the inactive part as one unit and uses the sum of their weight. The mass of the active part is 30 kg and that of the inactive part is 220 kg; and as such, gives a total rod mass of 250 kg (see Table 1).

2.2. Analysis conditions

From the primary LBE pump through the inlet the flow rate of LBE, flowing into the guide tube is estimated as 80.58 kg/s and the temperature of the incoming LBE is 350 °C (Arthur et al., 2020). The flow rate of LBE flowing through the inlet was assumed constant. The density and viscosity change of LBE due to the heat generated by the fuel rod and the impact of the drop velocity in the heating of the control rod was not considered due to the transient nature of the study. Since the drop is a freefall, rotation of the CRA will not occur during the fall and the moving CRA was assumed a one-dimensional translational motion in the direction of the gravitational force. With the CRA typically falling by gravity, the gravitational acceleration applied during the analysis is 9.81 m/s^2. Particularly for the analysis of this study, the domain requires three specifications. Firstly, the region defining the LBE fluid flow or the CRA/guide tube wall. The domain is formed from one or more 3D primitives that constraints the region occupied by the LBE fluid and CRA. Secondly, the physical nature of the LBE fluid flow determines the modelling of specific features such as buoyancy. Lastly, the properties of the materials in the region.

2.3. Analysis method

To analyse the phenomenon of the CRA drop dynamics due to gravity within the guide tube, the rigid body equations of motion was solved in conjunction with the flow equation that accounts for the LBE flow resistance inside the guide tube. This was done with the use of the CFX solver, which is a code, based on finite volume method (FVM). As the CRA drops, the generated grid is twisted and deformed continuously due to the sliding mesh technique and the deforming mesh technique that was used. In the model discretization, the tetrahedral mesh was generated for the analysis area that dealt with the deformation of the grid of the flow domain due to the moving CRA. To ensure accuracy of results, a dense grid in the expected area of deformation, the sliding surface position and the interface was constructed. It was observed that the size of each element on the face affected the results of the analysis. Therefore, by making the element size of the two sliding surfaces the same, and very small, the solution is sufficiently converged at each time step and as well, the magnitude of the error in the sliding surface is minimal.

The number of elements carefully chosen for the entire analysis domain is about 48,805 after a sensitivity analysis conducted (see Table 2) and Figure 2 is used to show the grid of the CRA. During operation of the reactor, the CRA is fixed in the reactor. However, the coolant flows at a constant rate via the bottom of the guide tube and in the CRA flow path to the top. To simulate the turbulence effect on the viscous term of the mass equation, the frequently used Reynolds-averaged Navier–Stokes (RANS) turbulence model called the standard, K-ε model was used because the model has proven useful for free-shear layer flow (Profir et al., 2015). Moreover, the time step for the

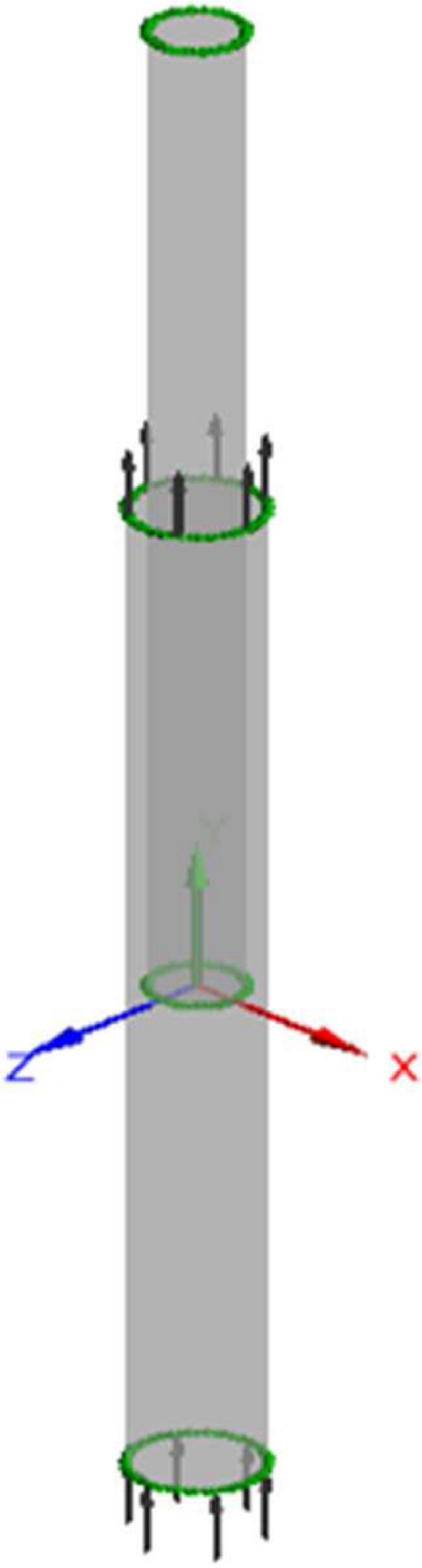

Figure 1. Simplified CRA geometry in 3-dimensions.

Table 1. Design parameters of the CRA and Guide tube.

Parameter	Value
Mass of CRA active part (kg)	30.0
Mass of CRA inactive part (kg)	220.0
CRA diameter (mm)	100.0
CRA active height (mm)	800.0
Guide tube diameter (mm)	141.5

transient analysis was set to 0.001 s. The discretization scheme used in the equation of motion and momentum is high-resolution advection scheme and second order backward Euler transient scheme. For the turbulence kinetic energy equation and dissipation rate, the upwind advection scheme and first order backward Euler transient scheme was used.

3. Results and discussion

3.1. Verification analysis

For verification, the CFD method being used was compared to the drop time and velocity ascertained from the theoretical approach under the normal operating conditions by Arthur et al. (2020).

The drop time ascertained from the theoretical approach under the normal operating conditions of the CLEAR-I is about 576.8 m (Arthur et al., 2020) and that ascertained from the CFD approach is about 585 m. This shows that there is a good agreement between the two approaches used for the study as a difference of 1.4 percent is observed between the two drop times as shown in Table 3.

3.2. CRA drop in the LBE environment under normal condition

Under the normal operating condition of the CLEAR-1, the weight of the CRA is about 2452.5 N as it drops under the acceleration due to gravity. The LBE fluid with density of 10,259 kg/m^3 flows at 80.58 kg/s into the guide tube from the inlet, which is located at the bottom and flows out from the top of the guide tube. The estimated total differential pressure is 5.55 kPa for the required flow of 80.58 kg/s in the CRA deposited position. To mimic exactly how the CLEAR-1 operates, the initial velocity and time was set to 0 m/s and 0 s respectively, whereas the initial position of the CRA was set to 800 mm. This means the CRA is 800 mm above the bottom of the guide tube where the CRA is supposed to end its fall. Therefore, at the end of the drop the CRA position is expected to be 0 m.

3.2.1. The relationship between CRA position and time

In Figure 3(a), it can be observed that the net force is very large at the beginning of the CRA motion. However, it decreases as the velocity of the CRA increases, and tends to approximately zero at the end, once the CRA reaches the terminal velocity. Initially when the drop is initiated, the fluid resistances are high and pushes the CRA up a bit until the CRA gains momentum through the LBE fluid. At the start of the CRA motion, the LBE resistance is high, which dramatically pushes up the CRA to a height of 800.01 mm, slowing down its motion. However, the CRA begins to gain momentum against the LBE resistances after a short time (about 8 m), when it is pushed up to a maximum height of about 800.13 mm away from its initial position of 800 mm. From this maximum height, it takes the CRA about 14 m to drop to reach its initial height (800 mm) and then continues in its drop process. By this time, the CRA has gained enough impelling force against the resistance of the LBE fluid. From Figure 3(a), when the CRA is dropped with the pressure difference (5.55 kPa) under the operating condition, the CRA reaches the maximum velocity of 2.79 m/s (see Figure 3(b)) during the drop. The computed drop time is 585 m.

Table 2. Mesh sensitivity.

Mesh	Elements	Drop Time (ms)	Computational Time (s)
A	**25415**	583.65	1015
B	**39904**	585.00	1916
C	**48805**	585.00	4904
D	**66008**	585.00	15500
E	**80142**	585.00	41200

Considerably, the pressure difference between the top and bottom ends of the guide tube causes upward flow of LBE against the CRA. This upward flow which ensures cooling also offers an amount of resistance against the drop of the CRA.

By principle, it can be observed from Figure 3(a) that the displacement-time curve has a changing slope. It is observed that the displacement curve is initiated with a very small slope and begins curving sharply (downwards) towards a large slope. The curve of changing slope is a sign of accelerated CRA motion (that is, changing velocity) resulting from the driving force. By applying the principle of slope, it is easy to conclude that the CRA displacement depicted by the curve is moving with a negative velocity (since the slope is negative) and this obeys the coordinate frame defined in the numerical simulation code used for this study. Furthermore, the CRA drop beginning with minimal velocity (the slope begins small) and ending with a large one (the slope becomes large) implies that the CRA is moving downwards with increasing speed (the small velocity turns into a larger velocity).

3.2.2. The relationship between velocity and time

The CRA in the LBE fluid undergoes a net upward buoyant force at the beginning of the drop process and bobs as it pushes into the LBE fluid. The buoyant force rises when the CRA pushes down as a result of increase in the volume of displaced coolant and the CRA experiences a net upward force. However, when the CRA bobs, less coolant is displaced to reduce the buoyant force to result in giving rise to a net downward force. This phenomena is explained by Figure 3(b) where the CRA velocity curve

Table 3. Comparison of the theoretical and CFD approaches.

Drop Characteristics	Theoretical (Arthur et al., 2020)	CFD
Drop time (ms)	576.8	585
Velocity (m/s)	2.81	1.79

falls from the time of initiating the drop until about 3 m. After this time, the velocity begins to increase steadily. Generally speaking, the magnitude of the buoyant force is proportional to the LBE coolant volume displaced by the CRA and militates against the velocity of the CRA. The velocity contours around the CRA at height of 800 mm for varying density are plotted in Figure 4. As expected, an area of high velocity is observed around the surface of the CRA. This high velocity is caused by the driving force. However, the velocity decreases with distance from the top of the CRA in downstream.

In the drop dynamics, the CRA drops at its terminal velocity for a constant speed because of the resistance exerted by the coolant through which the CRA drops. Considering the impacts of the buoyancy, the drop of the CRA (under its inherent mass) through the LBE coolant can attain a terminal velocity if the net force acting on the CRA approaches zero. Moreover, once the terminal velocity is achieved the CRA weight balances exactly with the upward buoyancy force and resistances of the LBE coolant.

3.3. LBE resistance on CRA movement

Under normal operating conditions, the differential pressure and viscous friction resistances with respect to position and time are depicted in Figure 5(a) and (b) respectively. Both the differential pressure and viscous friction resistances increase to militate against the driving forces of the CRA as it drops into the LBE fluid with position and time. However, the increase attains a maximum and reduces slightly before the drop is ended. For this case, the initial differential pressure and viscous friction resistances across the CRA are small at the beginning of the transient, but gradually increase substantially as the CRA gathers speed.

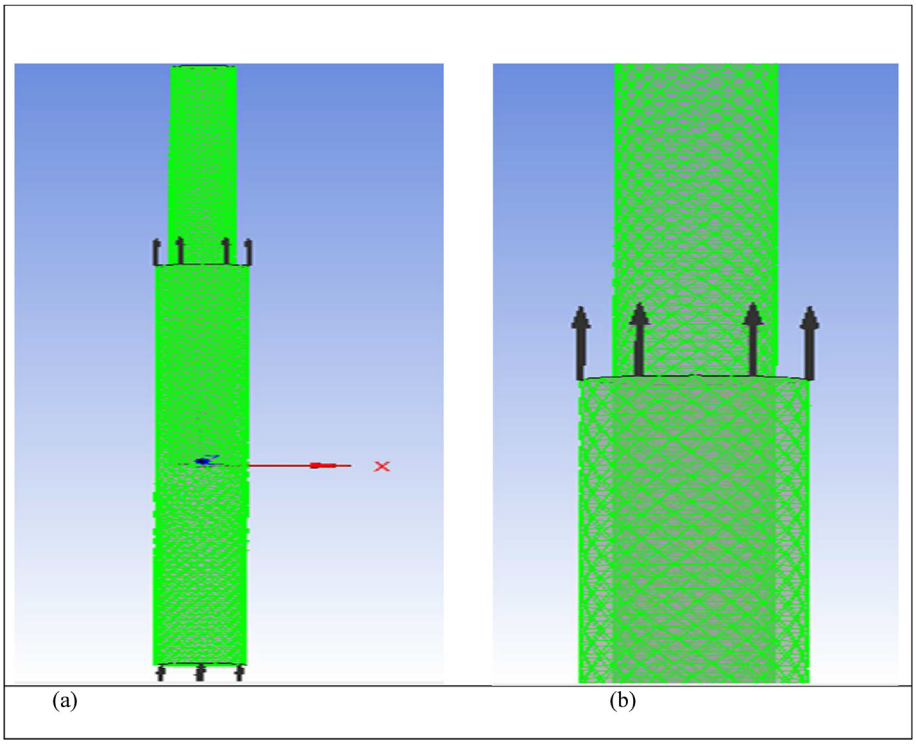

Figure 2. Model (a) grid and (b) partially enlarged view.

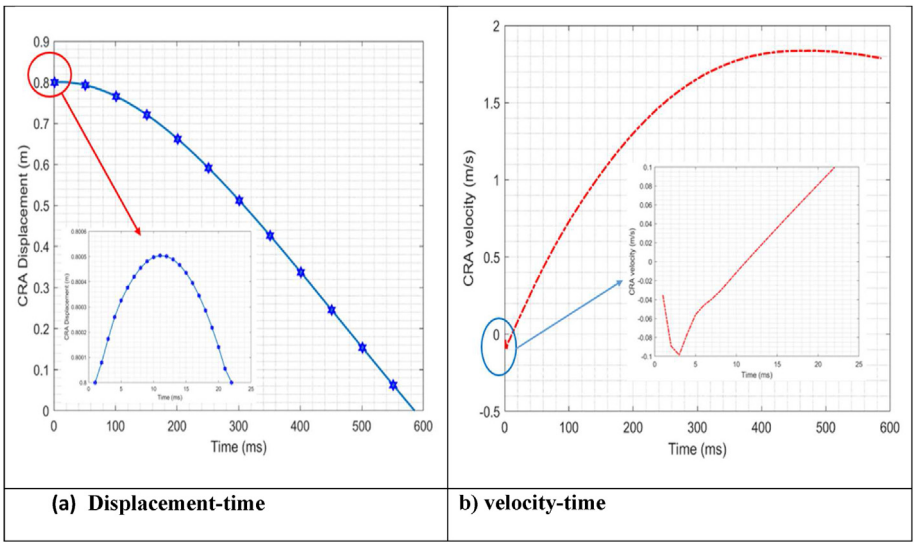

Figure 3. CRA drop in the LBE medium under normal conditions.

Therefore, the effect of higher initial acceleration is neutralised by the increased differential pressure and viscous friction resistances during the transient phase. Notably, in the process of the CRA drop both the viscous friction and the differential pressure resistances grow with time and at every position, the magnitude of the viscous friction resistance in the LBE fluid is higher than that of the differential pressure resistance. The viscous friction resistance exerted on the weight of the CRA as it drops typically relies on the speed of the CRA (contrary to simple friction). Notably, experimental works have demonstrated that for laminar flow, the viscous resistance is proportional to speed, whereas for turbulence, viscous resistance is proportional to the square of the relative speed. For the turbulent flow regime, the resistance increases dramatically and behaves with greater complexity (Rabiee and Atf, 2016). However, for the laminar flow regime, the viscous friction resistance is proportional to the LBE fluid viscosity, the CRA characteristic height as well as its velocity. All of which is plausible—the more viscous the LBE coolant and the higher the mass of CRA, the more resistance expected.

The pressure contours within the fluid domain at various time is represented in Figure 6. It is observed that an area of high pressure in the LBE can be detected at the bottom of the CRA. This area has a higher pressure as the CRA velocity increases. On the other hand, an area of low pressure at the outlet and a relatively high-pressure region can be observed in the wake of the CRA. The velocity of the moving CRA affects the pressure distribution in the LBE thus, as the CRA accelerates with time within the LBE fluid, the pressure in the LBE fluid increases until the CRA gets to a rest position. Additionally, it is observed that the maximum pressure distribution in the LBE fluid reduces with time as the CRA drops into LBE fluid. This can be explained by the fact that, with constant weight of the CRA, the pressure increases as the area of the CRA in the fluid increases. Thus, as the CRA pushes its way towards the bottom of the guide tube, the maximum pressure distribution which is normally seen beneath the falling CRA reduces.

The total resistance in the LBE against the driving force of the CRA during the drop process includes the viscous friction and differential pressure resistances as well as the buoyancy of the LBE fluid. In Figure 7(a), the total resistance in the LBE with position is depicted. It is observed that, the total resistance of the LBE increases exponentially as the CRA drops into the LBE fluid. This is anticipated because, the LBE resistance increases with the CRA velocity relative to the LBE flow. On the other hand, the total resistance in the LBE with time is depicted in Figure 7(b). It is observed that, at the start of the CRA drop, the LBE resistance increases exponentially with time and attains a maximum. The curve begins to fall slightly until it completes its trip at about 585 m.

Remarkably, comparing the graph of the total resistance of the LBE to the graph of viscous friction and differential pressure resistance (see Figures 5 and 7), it is observed that the magnitude of the total resistance

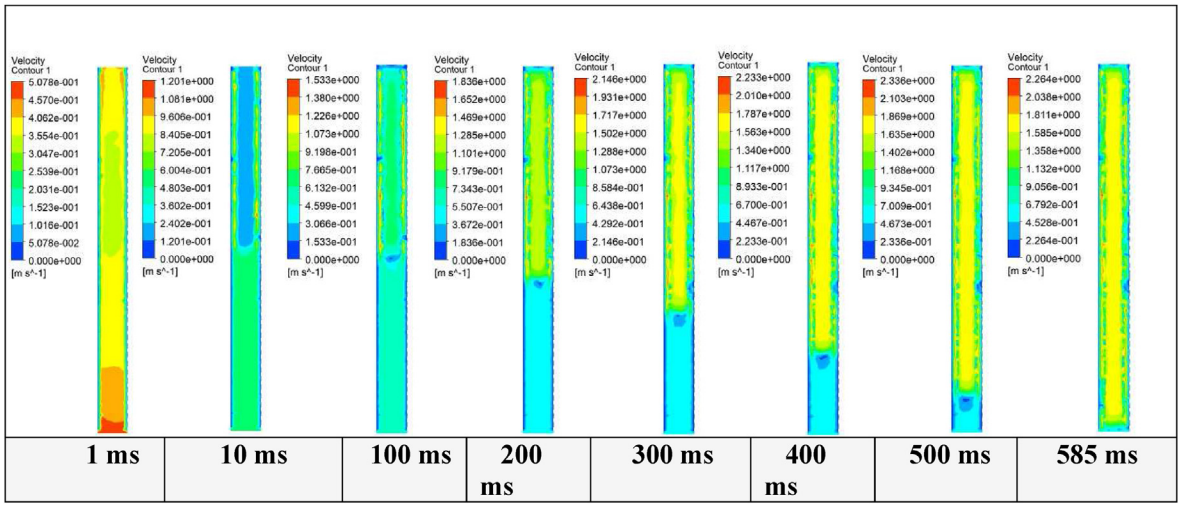

Figure 4. Velocity contour of CRA and LBE flow domains.

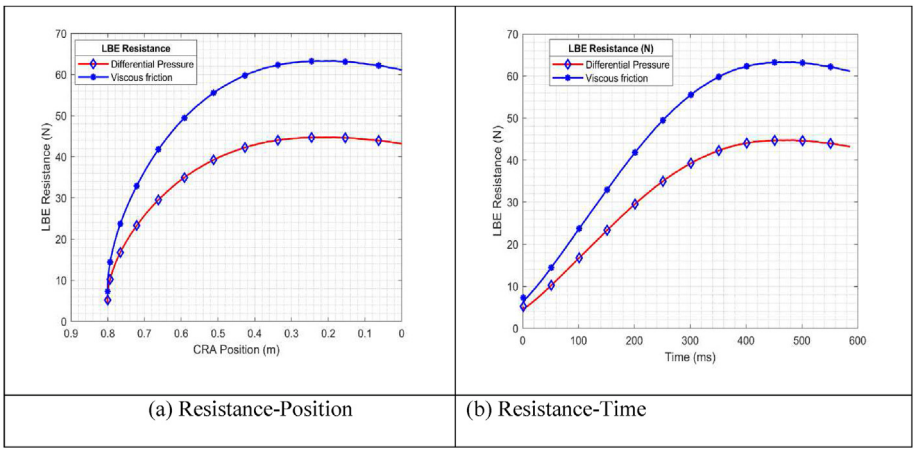

Figure 5. LBE Differential Pressure and viscous friction resistances against CRA drop.

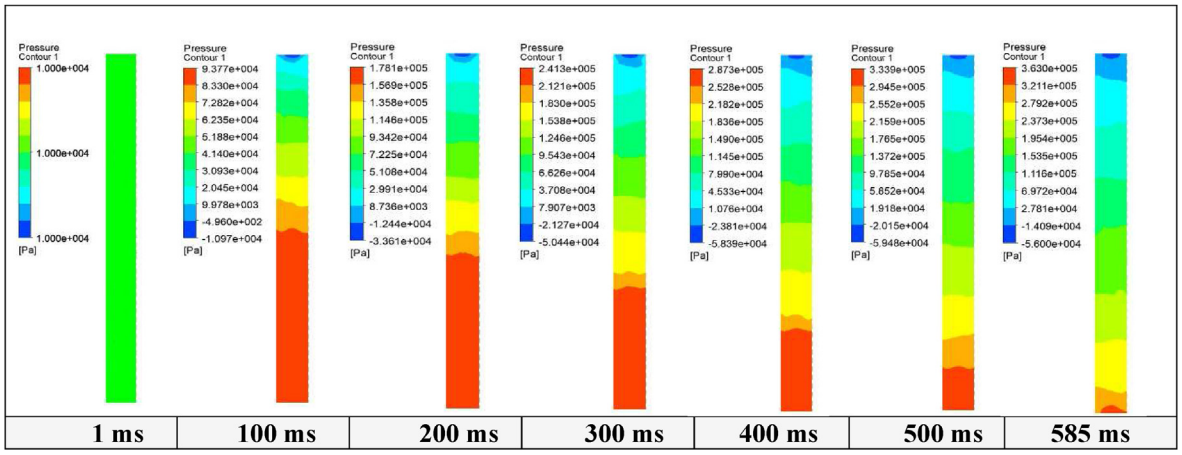

Figure 6. Pressure contour of the LBE flow domains.

is far higher than that of the viscous friction and the differential pressure resistances. This vast hike in the magnitude of the total LBE resistance is as a result of the inclusion of the resistance due to buoyancy of the LBE fluid which is also due to its extremely high density (about 10,258 kg/m^3). The magnitude of the resistance due to buoyancy of the LBE fluid against the driving force of the CRA alone is about 1264.7 N (see Figure 8) and the average values of the viscous friction and differential pressure resistances are 46.4 N and 32.8 N respectively. Clearly, the value of the buoyancy resistance is constant in time and will increase when the LBE density increases. Furthermore, the differential pressure and viscous friction resistances are transient terms which tend to zero once the motion of the CRA becomes steady. It is also clear that the differential pressure resistance is small, accounting for about 2.4 percent effect on the driving force and this is followed by the viscous friction resistance which also account for about 3.5 percent effect on the driving force of the CRA. However, the buoyancy of the LBE has larger contribution to the LBE resistance and accounts for about 94.4 percent effect on the driving force of the CRA, particularly in the accelerating phase of the motion. As expected the resistance force against the driving force of the CRA also increases as the velocity of the CRA increases. Moreover, it can be seen

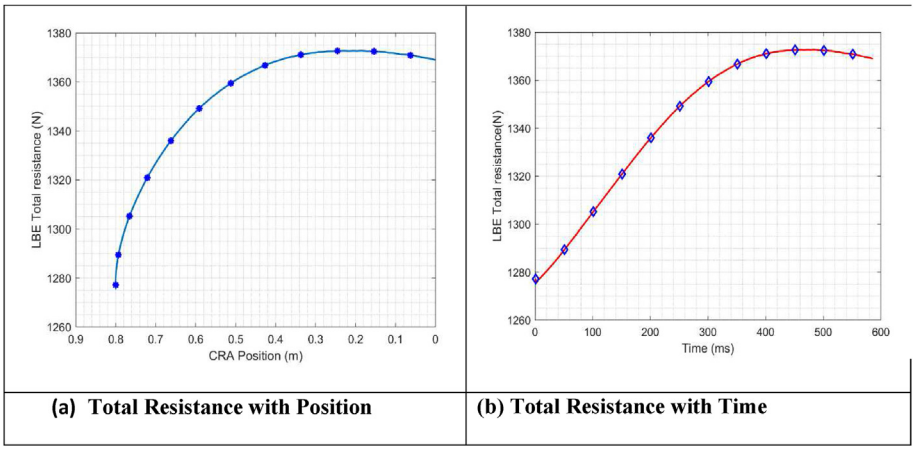

Figure 7. Total resistance of LBE against the CRA drop.

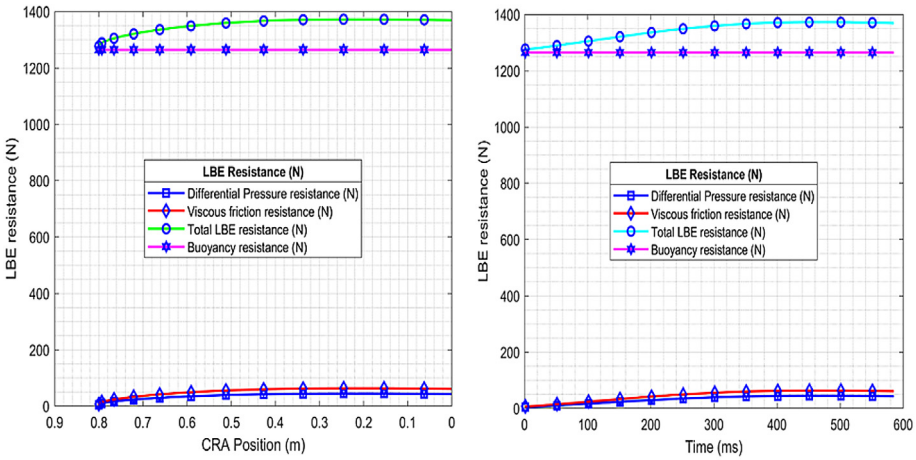

(a) LBE resistances with position **(b) LBE resistance with time**

Figure 8. LBE resistances during the CRA drop.

that the value of the resistance due to buoyancy remains constant (Figure 8(a) and (b)) throughout the LBE in the CRA drop process.

3.4. LBE mass flow rate variation on CRA drop

In the simplified model for the study, the guide tube has no bends and so form loss were not considered in the losses of the frictional model. In view of this, the mass flow rate in the guide tube is almost the same everywhere in the guide tube. Generally, knowing the effect of the mass flow rate on the drop time is very important because the direction of flow of the LBE from the down comer into the guide tube is against the direction of the CRA while it drops. A noteworthy relation is that the thermal power produced by a nuclear reactor directly relates the coolant flow rate as well as the temperature difference across the core. In terms of thermodynamic, the heat generation as well relates to the temperature difference of the coolant across the core and the flow rate of the coolant through the core. Therefore, reactor core size depends on and is limited by the mass of coolant that flows through the core.

3.4.1. The profiles of CRA position with time

In Figure 9(a), the CRA position with time for varying the LBE mass flow rate is presented. It can be seen that the various position curves for the given variation start at the same point and flattens for a distance of about 795 mm and detach after that time. As expected, the drop time is worsened for increasing magnitude of the LBE flow rate and the meaning to this as a result of the increasing mass flow rate can be found in the behaviour of the fluid resistance.

3.4.2. The profiles of CRA velocity with time

In Figure 9(b), the CRA velocity with time for varying mass flow rate of the LBE fluid is presented. It can be observed as the mass flow rate of the LBE increases, the velocity of the CRA reduces. In the CLEAR-I, the flow of the LBE into the guide tube is against the direction of the control rod, which means that as the CRA drops downward, the LBE fluid flows upward. This flow configuration increases the fluid resistance to reduce the terminal velocity and hence, increases the drop time.

3.4.3. The profiles of differential pressure resistance

The differential pressure resistance with position for varying LBE mass flow rate is depicted in Figure 10(a). It can be seen that as the LBE flow rate increases; the CRA does not get to enter the fluid easily as it bobs for a while before entering the fluid. This is a safety concern as a bit of delay is found at the initially stages when the drop is initiated, and this is part of what leads to a drop time increase for increasing mass flow rate. Moreover, with higher flow rates, the driving force of the CRA is resisted even halfway before getting close to the inlet where the resistance is also more. The resistance of the fluid due to differential pressure has effect on the CRA driving force and as has been seen, increases when the drop is

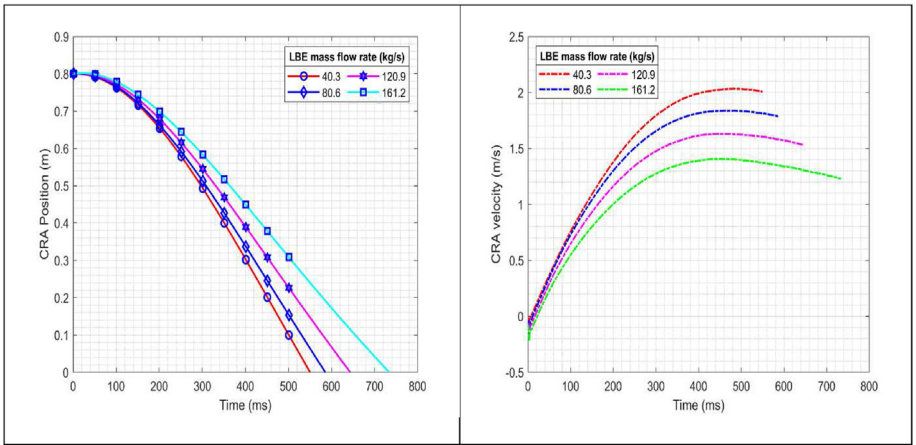

(a) Position with Time **(b) Velocity with Time**

Figure 9. LBE mass flow rate variation on the CRA drop time.

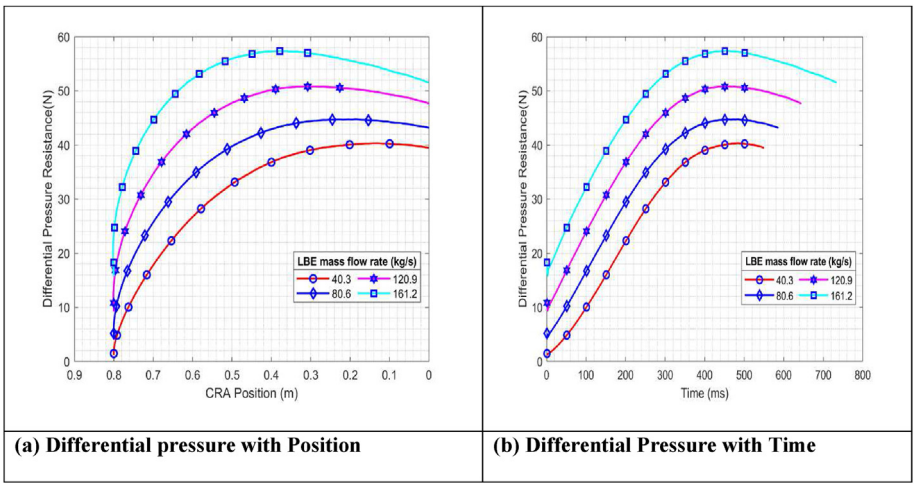

(a) Differential pressure with Position **(b) Differential Pressure with Time**

Figure 10. Differential pressure resistance with for varying mass flow rate.

initiated. The magnitude of the increase depends on the mass flow rate and the velocity of the CRA. At the initiating of the CRA drop, the magnitude of the differential pressure is what decides how high the CRA is pushed up before gaining momentum to drop into the LBE domain. Moreover, halfway of even before (depending on the magnitude of the mass flow rate) the CRA reaches the bottom, there is some decrease in resistance that is perhaps, caused by the flow of the fluid from the inlet. Thus, as the CRA gets to the end of the trip, the resistance due to differential pressure keeps reducing as the CRA velocity reduces. This eventually causes a high drop time of the CRA.

3.4.4. The profiles of viscous friction resistance

In Figure 11(a), the viscous friction resistance with position as the CRA drops the guide tube for varying mass flow rate is presented. The delays in the drop time from the viscous resistance due to increasing mass flow rate is obvious as the delay starts from the beginning of the drop and somewhere during the drop where the resistance has reached its maximum. At high mass flow rate, the viscous friction resistance is high immediately the drop is initiated and that contributes to the bob of the CRA. Therefore, there is some time spent by the CRA to gather momentum to drop down into the LBE fluid. Moreover, when the CRA had entered the LBE fluid domain with the driving force while accelerating, the viscous friction resistance increases rapidly until it gets to a maximum to slow down the CRA. For a low flow rate, this happens at the point where the CRA approaches the end of the trip. However, as the mass flow rate increases further, the maximum viscous friction resistance is seen halfway or less, in the CRA drop.

A notable result from the increase in the LBE viscous friction resistance against the CRA speed is that, in dropping through the LBE coolant, the CRA will not continue to indefinitely accelerate (as this is possible if the LBE resistance is neglected). Rather, viscous friction resistance rises to slow the CRA acceleration until it approaches zero and a terminal speed (also called the critical speed) is reached. As soon as this occurs, the CRA continues to fall at constant speed (the terminal speed). There is a viscous friction resistance on the CRA that depends on the viscosity of the fluid and the differential pressure resistance as well as the size of the CRA. Nevertheless, also a buoyant force is dependent on the density of the CRA relative to the LBE coolant. However, the terminal velocity will be maximum for low-viscosity fluids and high density CRA with small base area.

The mass flow rate has direct effect on the differential pressure resistance and the viscous friction resistance than on the buoyancy resistance. In that case, the variation in the total resistance in the LBE with position and time when the mass flow rate is varied comes because of the variation in the resistance due to differential pressure and viscous resistance. When the mass flow rate is increased, the initial observation is the buoyancy that pushes the CRA up for a while and thereafter, it is released to drop, the pressure difference and viscous friction resistances coming into play. However, at high mass flow rate, the total resistance at the start of the drop is high and its effects contributes to the delay of the

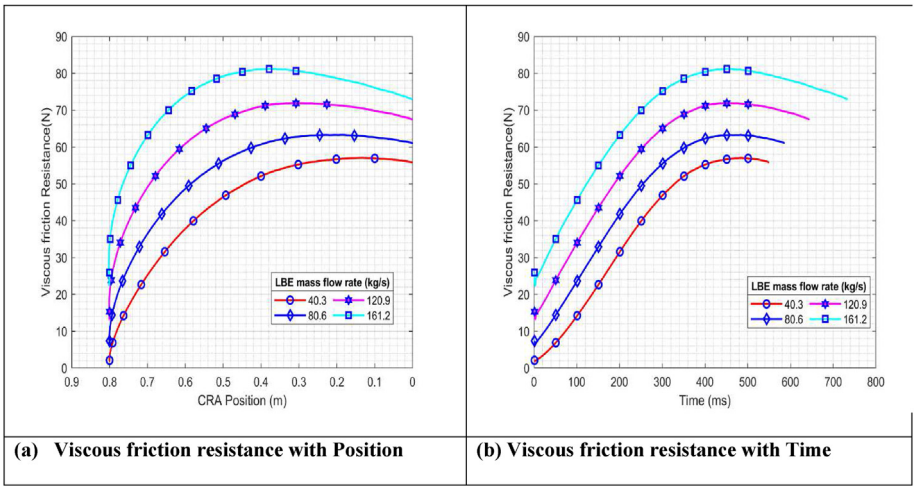

(a) Viscous friction resistance with Position **(b) Viscous friction resistance with Time**

Figure 11. Viscous friction resistance for varying mass flow rate.

CRA drop by pushing it to a significant height before starting to drop. Moreover, while dropping, because the mass flow rate is high, the maximum resistance of LBE is also high and slows the CRA before getting to the end of the drop. The effect is an increase in the drop time of the CRA, which is a safety concern. The behaviour of the LBE resistance due to the mass flow rate variation is very necessary in the nuclear reactor operation. This is because the heat transfer at the core of the reactor is dependent on the mass flow rate of the coolant, among other factors. A considerable magnitude of the flow rate of the coolant is needed to take away the heat accumulated in the primary loop. However, the flow rate is also directly proportional to the resistance that militates against the driving force of the CRA. Therefore, choosing the appropriate mass flow rate of the coolant is a gamble between heat transfer and CRA drop time quality.

3.5. CRA mass variation on the CRA drop in the LBE medium

3.5.1. The profiles of CRA position with time

The position of the CRA with time for varying the CRA mass during the drop process is shown in Figure 12(a). It is observed that the increase in the mass of the CRA has some influence on the drop time, as it is a contributing factor that drives the CRA. In other words, the weight of the CRA is the product of the mass of the CRA and the gravitational acceleration. Thus, the driving force is a function of the mass of the CRA. In that case, as the mass of the CRA increases, although the CRA bobs to height, the waiting time there is minimal as well as the maximum height at which the CRA is pushed up. Consequently, the more the mass of the CRA the less time it takes the CRA to drop into the core and the converse is true.

3.5.2. The profiles of velocity with time

It has been gathered that when the mass of the CRA increases the driving force increases and the velocity of the CRA increases significantly. Remarkably, when the CRA mass was 125 kg and 250 kg, the LBE resistance reduces the maximum velocity but at a mass of 375 kg and 500 kg, the maximum velocity is maintained until the end of the drop (see Figure 12(b)). Nevertheless, the increase in the driving force of the CRA as a result of the increased mass of the CRA leads to the increase in the terminal velocity and hence, a decrease in the drop time of the CRA. In the CLEAR-1 architecture, the diameter of the CRA is about 70.7 percent of the guide tube diameter and this means the CRA can enter the guide tube with leaving some annular region at the sides after displacing the fluid. The CRA diameter is not large enough to achieve certain mass that can still help in an easy drop, thus for the CLEAR-1 a counterweight is added on top of the active part of the CRA to make the drop possible.

3.5.3. The profiles of differential pressure resistance

In Figure 13(a), the LBE differential pressure resistance with position for varying CRA mass is depicted. It is observed that the differential pressure resistance is related to the velocity of the CRA, and the differential pressure has adverse effect on the CRA as it accelerates. As the CRA mass is increased, the velocity of the CRA increases which increases the differential pressure resistance but unfortunately, the driving forces increase more than proportionately as compared with the LBE resistance. Therefore, the resistance due to differential pressure is not able to slow the CRA down significantly during the drop and gains a higher magnitude rather at the end of the drop. When the weight of the CRA is more, say 375 kg or more, the drop does not face any disturbances arising from the differential pressure resistance and this enables the CRA to keep an increasing velocity until the end of the drop. In effect, the drop time can be kept well within an acceptable range to ensure the safety of the nuclear reactor operation.

Figure 13(b) shows the differential pressure resistance with time as the CRA mass varies. The distribution of the differential pressure resistance with time and position in the drop process of the CRA is not constant but rather depends on the magnitude of the CRA mass. When the CRA mass is high, the differential pressure force increases due to increased weight. The increased weight affects the driving force to increase the acceleration of the CRA. In that case, the CRA does not take much time to get to a given position in the LBE-filled guide tube. Although at the beginning of time, the CRA bobs despite its increased weight, the LBE fluid is not able to hold the CRA for far too long before dropping. Notably, the differential pressure resistance of the 125 kg curve tends to be constant due to its speed gradually approaching a uniform speed. However, for the 250 kg, 375 kg and 500 kg curves, the resistance curve will increase due to the continuous increase in speed. The slope of the change increases continuously and this is because the differential pressure resistance changes with the square of the speed, but the increase in the slope also shows a decreasing trend with the decrease in the increase in speed.

3.5.4. The profiles of viscous friction resistance

In Figure 14(a), the LBE viscous friction resistance with position for varying CRA mass is depicted. It is seen that the viscous friction resistance distribution of the CRA at a given position while the CRA drops is observed to be affected by the mass of the CRA. The viscous friction resistance curves over time for varying the CRA mass increase differently based on the mass of the CRA. The CRA increases to increase its velocity and when the velocity is increasing, the relative velocity between the fluid increases and increases the viscous friction resistance of the LBE fluid. When the CRA mass is below 250 kg, it is observed that getting to the midway to the drop time or even less, the viscous friction resistance attains a maximum and begins to reduce until the drop is ended.

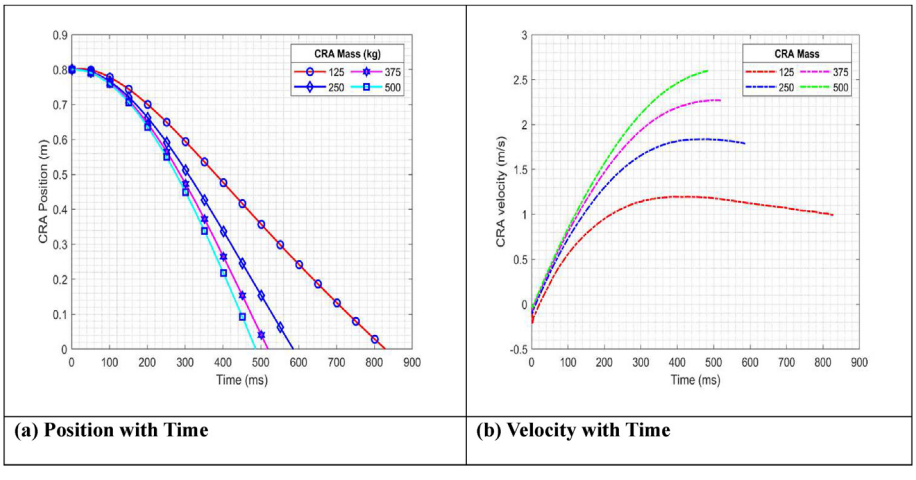

(a) Position with Time (b) Velocity with Time

Figure 12. CRA mass variation on the drop time.

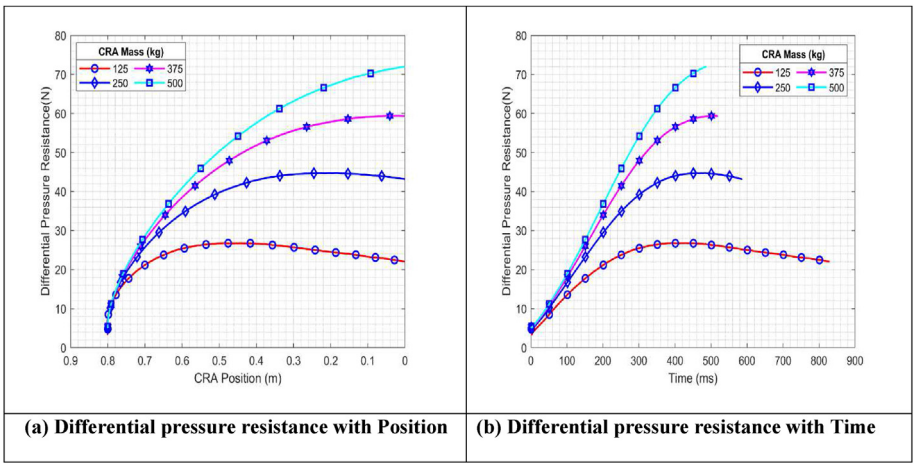

(a) Differential pressure resistance with Position (b) Differential pressure resistance with Time

Figure 13. Differential pressure resistance for varying CRA mass.

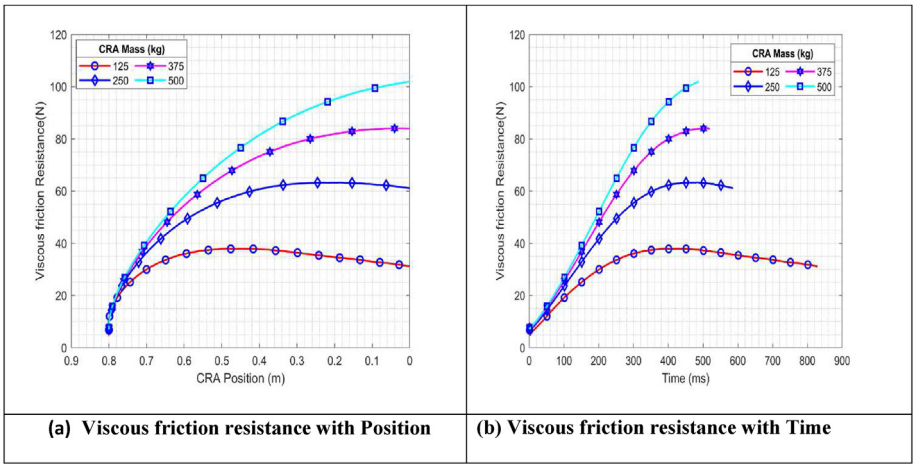

(a) Viscous friction resistance with Position (b) Viscous friction resistance with Time

Figure 14. Viscous friction resistance for varying CRA mass.

However, for a CRA mass above the 250 kg, the viscous friction resistance attains the maximum either close to the end or at the end of the drop and reduces until the end of the drop.

The distribution of the differential pressure resistance with time and position in the drop process of the CRA is not constant but rather depends on the magnitude of the CRA mass. When the CRA mass is high, the differential pressure force increases due to increased weight. The increased weight affects the driving force to increase the acceleration of the CRA. In that case, the CRA does not take much time to get to a given position in the LBE-filled guide tube. Although at the beginning of time, the CRA bobs despite its increased weight, the LBE fluid is not able to hold the CRA for far too long before dropping. Notably, the differential pressure resistance of the 125 kg curve tends to be constant due to its speed gradually approaching a uniform speed. However, for the 250 kg, 375 kg and 500 kg curves, the resistance curve will increase due to the continuous increase in speed. The slope of the change increases continuously and this is because the differential pressure resistance changes with the square of the speed, but the increase in the slope also shows a decreasing trend with the decrease in the increase in speed.

It can be seen that the 300 kg CRA drop curve, the change trend is the same but gentler. The disturbance of LBE flow resistance is more obvious for low rod mass, thus, when the total mass of the CRA is 125 kg, it cannot meet the safety requirements. However, as a comparison, it was revealed intuitively that the resistance time curve gradually changes from a parabolic form with time and approaches a straight line. This is due to the gradual increase of buoyancy, differential pressure resistance and viscous frictional resistance. In the mid part of the drop, the force reaches equilibrium with the mass of the CRA, the acceleration approaches 0, and the CRA moves at a constant speed. In addition, under normal conditions, the increase of gravity affects the slope of displacement with time curve and as the CRA weight increases, the initial acceleration gradually approaches the acceleration due to gravity the degree of the influence of the CRA mass gradually decreases. This is because in the case of the high mass of the CRA, the influence of the LBE resistance from the mass flow rate is relatively small. When the mass of the control rod decreases, the influence of the LBE resistance from the mass flow rate begins to manifest.

4. Conclusion

The CLEAR-I is one of the Chinese technology archetypes for the lead-cooled fast reactors (LFR) which marks the leading edge of the Accelerator Driven Subcritical (ADS) transformation system of the Chinese Academy of Sciences (CAS). To study the CRA drop of CLEAR-I under gravity within the guide tube, the rigid body equation of motion was coupled with the flow equation that accounts for the LBE flow resistance inside the guide tube. These equations were solved with the finite volume method (FVM) based ANSYS CFX solver. Using the sliding mesh and deforming mesh techniques, the generated grid is twisted and deformed continuously as the control rod drops into the LBE coolant in the guide tube. From the simulation, the relationship between time, displacement, velocity as well as resistance against the drop of the CRA and vital safety variables including the drop time and velocity of the CRA were found. The CFD

analysis done has been carefully fashioned to mimic the exact test section for the study and the result generated is concluded as follows:

The drop time of the CRA ascertained during the normal operating conditions is 585 m at a final velocity of 1.79 m/s. In the LBE fluid, the difference in the pressure at the inlet and outlet of the guide tube creates an upward flow against the CRA. The purpose of this is ensuring cooling in the reactor core; however, this militates against the free fall of the CRA by offering a considerable resistance in the LBE. The CFD results have shown that the mass density contributes most to the resistance capability of the LBE fluid. Notwithstanding, the share of the resistance from viscous friction and differential pressure cannot be underestimated. In the drop process of the CRA in LBE domain, the fluid solid interaction capability of the CFX software can show the actual characteristics of the CRA drop in response to the LBE resistance. It has been shown that at the beginning of the drop, the LBE resistance increases and the CRA bobs and this causes a delay, which is a safety concern. For the controlling parameters from the LBE fluid, increasing the density and mass flow rate causes a corresponding increase in the drop time as these parameters contribute to increasing the resistance against the driving force of the CRA.

However, the controlling parameter from the CRA is the mass and as this mass increases, the drop time reduces. In case of the CRA drop, the study shows that the change in the drop time is because of the variation of the fluid resistance due to buoyancy, differential pressure and viscous friction caused by the variation in the LBE controlling parameters.

Analysis of the hydraulic resistance is one of the most important analyses in designing a CRA and analysing the hydraulic compatibility of mixed cores. The vertical forces are induced by upward high-velocity flow through the reactor core. Essentially, the CRA provides real-time control of the fission process, ensuring that it remains active while preventing it from accelerating out of control. In effect, control rods are an important safety system of nuclear reactors. Their prompt action and prompt response of the reactor is indispensable. The behaviour of the total resistance with time is worth studying as it shows the behaviour of the CRA because of the resistive effect of the LBE at any point in time, during the drop process.

Finally, the numerical study on the drop dynamics of the CRA done in this work is therefore conservative and represents the CLEAR-1 conditions adequately. It is also appropriate for showing the principle behind the control rod drop dynamics as well as contribute to the qualification of the CLEAR-I control rod design.

Declarations

Author contribution statement

Emmanuel Maurice Arthur: Performed the experiments; Analyzed and interpreted the data; Wrote the paper.

Chaodong Zhang: Conceived and designed the experiments; Performed the experiments; Analyzed and interpreted the data; Contributed materials, analysis tools or data; Wrote the paper.

Seth Kofi Debrah: Conceived and designed the experiments; Performed the experiments; Analyzed and interpreted the data.

Stephen Yamoah: Performed the experiments; Analyzed and interpreted the data.

Lei Wang: Conceived and designed the experiments; Performed the experiments; Analyzed and interpreted the data; Contributed materials, analysis tools or data.

Funding statement

This work was supported by the Strategic Priority Research Program of Chinese Academy of Sciences (Grant No. XDA22010504).

Data availability statement

Data will be made available on request.

Declaration of interests statement

The authors declare no conflict of interest.

Additional information

No additional information is available for this paper.

Acknowledgements

The authors are grateful to the reviewers for their intelligible critique to the substance of the study.

References

Arthur, E.M., Zhang, C., Debrah, S.K., Yamoah, S., Wang, L., 2020. Analysis of the drop dynamics of control rod assembly in a LBE-cooledresearch reactor. Ann. Nucl. Energy 149.

Cheng, J., Wang, Z., Lu, C., Zhang, J., Bi, S., Feng, Q., 2020. Control rod drop hydrodynamic analysis based on numerical simulation. Front. Energy Res. 8, 342.

Ferrini, M., Borreani, W., Lomonaco, G., Magugliani, F., 2016. Design by theoretical and CFD analyses of a multi-blade screw pump evolving liquid lead for a Generation IV LFR. Nucl. Eng. Des. 297, 276–290.

Hofmann, F., Archambeau, F., Chaize, C., 2000. Computational fluid dynamic analysis of a guide tube in a PWR. Nucl. Eng. Des. 200 (1), 117–126.

Huang, H., Wang, Z., Xu, W., Liu, T., Yang, Y., Li, P., 2018. Seismic analysis of PWR control rod drop with the CRDAC scram performance code. Ann. Nucl. Energy 114, 624–633.

Huh, H., Cho, Y.G., Choi, M.H., Kim, J.I.H., Kim, J.I., 2011. he Design, Fabrication , and Characteristic Experiment of the Electromagnet of Bottom-Mounted Control Rod Drive Mechanism for Research Reactor. In: T, pp. 69–70.

Huh, H., Cho, Y., Kim, J., 2013. Magnetic Actuation Connector between Extension Shaft and Armature for Bottom Mounted Control Rod Drive Mechanism, pp. 3–4.

Huh, H., Choi, M.H., Yu, J.Y., Cho, Y.G., Kim, J.I., 2010. Analysis on Electromagnetic Characteristics of the Research reactor control rod drive mechanism for thrust force improvement. In: Transactions of Korean Nuclear Society Autumn Meeting, Jeju, Korea, October 21-22, pp. 101–102.

Huh, H., Lee, J., Kim, S., Choo, Y., Sun, J., Lee, H., Yoo, Y., Kim, K., 2018. A Study on Improvement of Initial Drop Time for Bottom-Mounted Control Rod Drive Mechanism with a Hybrid Type Electromagnet in a Upward Flow Research Reactor, pp. 17–18.

Kim, J., Yoon, K., Oh, S.-H., Ko, S., 2015. CFD analysis to estimate drop time and impact velocity of a control rod assembly in the sodium cooled faster reactor. KSFM J. Fluid Mach. 18 (6), 5–11.

Kim, K.-R., Jang, K.-J., Park, J.-S., Lee, W.-J., 2011. Drop time evaluation for SMART control rod assembly. J. Fluid Mach. 14 (2), 25–28.

Lee, H.S., Yoon, K.H., Kim, H.K., Cheon, J.S., Lee, C.B., 2016. Drop Impact Analysis of Control Rod Assembly for Sodium-Cooled Fast Reactor.

Lee, Hyun Seung, Yoon, K.H., Kim, H.K., Cheon, J.S., Lee, C.B., 2017. Integrity evaluation of control rod assembly for sodium-cooled fast reactor due to drop impact. Trans. Korean Soc. Mech. Eng., A 41 (3), 233–239.

Oh, S., Kim, J., Yoon, K., Choi, C., Son, S., 2015. Numerical Analysis on the Free Fall Motion of the Control Rod Assembly, pp. 4–7.

Peng, S.J., Zhou, C., Yu, C.G., 2012. The numerical simulation of three-dimensional dynamic-mesh flow field of a hydraulic buffer. Adv. Mater. Res. 588, 1264–1268.

Profir, M., Moreau, V., Kennedy, G., 2015. Numerical analysis of MYRRHA control rod system dynamics. In: International Topical Meeting on Nuclear Reactor Thermal Hydraulics 2015, NURETH 2015, vol. 6, pp. 4717–4730.

Profir, Manuela, Graham, K., Vincent, M., 2017. Proof-of-principle of the control rod emergency insertion in the myrrha nuclear facility from a combined numerical-experimental campaign centre for advanced studies. In: Research and Development in Sardinia (CRS4), Italy Belgian Nuclear Research Centre (S. Journal of Nuclear Research and Development), 14.

Rabiee, A., Atf, A., 2016. Control rod drop hydrodynamic analysis for a pressurized water reactor. Prog. Nucl. Energy 88, 191–197.

Singh, N.K., Badodkar, D.N., Singh, M., 2014. Numerical and experimental study of hydraulic dashpot used in the shut-off rod drive mechanism of a nuclear reactor. Nucl. Eng. Des. 273, 469–482.

Son, J.G., Lee, J.H., Kim, H.W., Kim, S.K., Kim, J.B., 2019. Influence of design modification of control rod assembly for Prototype Generation IV Sodium-cooled Fast Reactor on drop performance. Nucl. Eng. Technol. 51 (3), 922–929.

Sui, H., Li, P.F., Ma, S.H., Ma, F.Y., Hu, Y., 2013. Proficient in CFD Dynamic Grid Engineering Simulation and Case Practice. People's Post and Telecommunications Publishing House, Beijing, China.

Sun, J., Kim, G., Yoo, Y., Cho, Y., In, J., 2014. Design of Seismic Test Rig for Control Rod Drive Mechanism of Jordan Research & Training Reactor.

Wu, Y., Bai, Y., Song, Y., Huang, Q., Zhao, Z., Hu, L., 2016. Annals of nuclear energy development strategy and conceptual design of China lead-based research reactor Chinese Academy of Sciences. Ann. Nucl. Energy 87, 511–516.

Yoon, K.H., Kim, J.Y., Lee, K.H., Lee, Y.H., Kim, H.K., 2007. Application of ADINA Code for Control Rod Drop Analysis, pp. 25–26.

Zhou, X., Mao, F., Min, P., Lin, S., 2013. Calculation of drop course of control rod assembly in PWR. Atomic Energy Sci. Technol. 47 (9), 1584–1589.